CrystEngComm

Accepted Manuscript

ROYAL SOCIETY OF CHEMISTRY

www.rsc.org/crystengcomm

Two 3D metal-organic frameworks of Cd(II): Modulation of structures and porous properties based on linker functionalities

Ritesh Haldar,[a] Satyanarayana Bonakala,[b] Prakash Kanoo,[b] Sundaram Balasubramanian,[b*] Tapas Kumar Maji[ab*]

[a]*New Chemistry Unit, Jawaharlal Nehru Centre for Advanced Scientific Research, Jakkur, Bangalore 560 064, India.*

[b]*Chemistry and Physics of Materials Unit, Jawaharlal Nehru Centre for Advanced Scientific Research, Jakkur, Bangalore 560 064, India.*

Abstract: Two new Cd(II) based metal-organic frameworks (MOFs), {[Cd(NH_2-bdc)(bpe)]·0.5EtOH}$_n$ **(1)** and {[Cd(NO_2-bdc)(azbpy)]·4H_2O}$_n$ (**2**) (NH_2-bdc = 2-amino terepthalic acid, bpe = 1,2-bispyridylethane, NO_2-bdc = 2-nitro terepthalic acid, azbpy = 4,4′-azobipyridine) have been synthesized by solvent diffusion technique and structurally characterized. Both the frameworks are constructed based on exo-bidentate pyridyl type linkers of similar length but different functionalities. Compound **1** has a 3D structure in which the –NH_2 functional group of NH_2-bdc is coordinated to Cd(II) and a 1D ultra-micropore accommodates ethanol guest molecules. Desolvated framework of **1** (**1′**) is rigid as realized from the PXRD patterns and shows a type-I CO_2 uptake profile with reasonably high isosteric heat of adsorption value. Density functional theory (DFT) calculation shows aromatic π electrons interact strongly with CO_2 and the binding energy is 33.4 kJmol^{-1}. Compound **2** has a two-fold interpenetrated 3D porous framework structure where pendent –NO_2 groups of NO_2-bdc are aligned on the pore surface. The desolvated framework (**2′**) exhibits structural transformation and is nonporous to N_2. Smaller and gradual CO_2 uptake in **2′** can be attributed to the structural contraction. The solvent (H_2O, MeOH and EtOH) vapour adsorption studies suggest pore surface of **2′** is hydrophobic in nature.

Introduction

Metal-organic frameworks (MOFs) or porous coordination polymers (PCPs) are attractive candidates for functional applications such as gas storage,[1] separation,[2] catalysis,[3] molecular sensing[4] and in opto-electronics due to their modular nature.[5] Rational design and synthesis of MOFs with a targeted application would be accomplished based on a self-assembly process of metal ions and linkers with needed functionalities. Various configurations or conformations of organic linkers have been exploited to get novel structural topologies, tuneable surface areas and related properties.[6] Comparison with other porous materials such as porous carbon[7] and zeolites[8], MOFs are far more promising due to their very high surface area and structural flexibility.[9] Therefore the structural modulation of MOFs is a key parameter for developing new functional materials. Recent studies by climate scientists suggest that increase in the atmospheric concentration of CO_2 has significant impact in the global environment and climate change. Post combustion flue gas from coal-fired power plant is a major source of CO_2; therefore selective capture of CO_2 with high CO_2/N_2 selectivity is of paramount importance as the flue gas contains more than 80% N_2. Such selectivity can be achieved based on modification of the pore surfaces and several approaches have been implemented in MOFs such as presence of unsaturated metal sites, incorporation of organic linkers with $–NH_2$, -OH, -F functionalities for selective interactions with CO_2.[10] Furthermore, additional functionalities ($-NH_2$, -OH, $-NO_2$, -SH, $-SO_3H$) in the backbone of aromatic dicarboxylates or pyridyl based linkers can endow structural diversity and complexity as such functional groups can also coordinate with the metal center.[11] Our group has been extensively working on design and synthesis such framework structures with potential applications in selective CO_2 uptake properties.[3c,12]

In the present work, we study such functionalized organic linkers to see its impact on the structure and functionality. We have chosen two functionalized terephthalate linkers, 2-amino terepthalic acid (NH_2-bdc) and 2-nitro terepthalic acid (NO_2-bdc) to construct two 3D MOFs; $\{[Cd(NH_2\text{-bdc})(bpe)]\cdot 0.5EtOH\}_n$ **(1)** and $\{[Cd(NO_2\text{-bdc})(azbpy)]\cdot 4H_2O\}_n$ (**2**). The -NH_2 group of NH_2-bdc linker coordinates to the metal center while -NO_2 group of NO_2-bdc remains pendent. Compound **1**, a rigid 3D porous structure, adsorbs CO_2 selectively over N_2 at 195 K and theoretical studies suggest that aromatic π clouds of the linkers interact with the CO_2 molecules in the pore surfaces. In case of **2**, pendent NO_2 group remains aligned along the pore channels but do not show significant CO_2 uptake properties. This can be attributed to the structural contraction as realized by the PXRD studies. Presence of aromatic rings in the

pore walls imposes hydrophobicity which is reflected in the solvent (H_2O, MeOH and EtOH) vapour adsorption properties.

Experimental

Materials

All the reagents employed were commercially available and used as provided without further purification. $Cd(NO_3)_2 \cdot 6H_2O$ was obtained from Spectrochem, 1,2-bis(4-pyridyl)ethane was obtained from Sigma Aldrich chemicals. 4,4′-Azobipyridine was synthesized following literature reported procedure.[13]

Physical Measurements

The elemental analysis was carried out using a Thermo Fischer Flash 2000 Elemental Analyzer. IR spectra were recorded on a Bruker IFS 66v/S spectrophotometer using KBr pellets in the region 4000-400 cm^{-1} with 10 scans for each measurement. Thermogravimetric analysis (TGA) were carried out (Metler Toledo) in nitrogen atmosphere (flow rate = 50 ml min^{-1}) in the temperature range 30 – 500 °C (heating rate = 3°C min^{-1}). Powder XRD patterns of the compounds in different states were recorded by using Cu-K_α radiation (Bruker D8 Discover; 40 kV, 30 Ma).

Synthesis of $\{[Cd(NH_2\text{-}bdc)(bpe)]\cdot 0.5EtOH\}_n$ (1)

$Cd(NO_3)_2 \cdot 6H_2O$ (0.5 mmol, 0.154 g) was dissolved in 25 mL of water. An aqueous solution (5 mL) of 2-amino benzenedicarboxylic acid (NH_2-bdc) (0.5 mmol, 0.112 g) was mixed with an ethanolic solution (20 mL) of 1,2-bispyridylethane (bpe) (0.5 mmol, 0.092 g) and stirred for 30 min to mix well. 2 mL of this ligand solution was layered over metal solution carefully and left undisturbed for 30 days. Colourless rectangular shaped crystals were isolated and washed with ethanol before single-crystal X-ray diffraction measurement. Bulk compound was prepared by direct mixing of the corresponding ligand and metal solution. Compound **1**: Yield: 68%, relative to Cd. FT-IR (KBr pellet, 4000-400 cm^{-1}): 3492(b), 3234(w), 3070(w), 2330(s), 2232(m), 2126(m), 1610(s), 1568(s), 1502(s), 1424(s), 1311(w), 1223(s), 1065(s), 1021(s), 910(w), 872(w), 829(s). Anal.Calcd. for $C_{22}H_{23}CdN_3O_5$: C, 50.85; H, 4.40; N, 8.05. Found: C, 51.11; H, 4.27; N, 8.19.

Synthesis of {[Cd(NO_2-bdc)(azbpy)]·4H_2O}$_n$(2)

A DMF solution (5 mL) of 2-nitro-benzenedicarboxylic acid (NO_2-bdc) (0.5 mmol, 0.1055 g) was mixed with a 2-methoxyethanol solution (20 mL) of 4,4′-azobipyridine (azbpy) (0.5 mmol, 0.092 g) and stirred for 30 min to mix well. $Cd(NO_3)_2·6H_2O$ (0.5 mmol, 0.154 gm) was dissolved in 25 mL of methanol and 2 mL of this metal solution was layered over above mentioned ligand solution. After 15-20 days red colour rectangular shaped crystals were isolated and washed with methanol before taking for single-crystal X-ray diffraction. Bulk compound was prepared by direct mixing of the corresponding ligand and metal solution. Compound **2**: Yield: 57%, relative to Cd. FT-IR (KBr pellet, 4000-400 cm^{-1}): 3499(b), 3251(w), 3089(w), 2341(s), 1618(s), 1587(s), 1497(s), 1365(w), 1256(s), 1013(s), 926(w), 856(w), 822(s). Anal.Calcd. for $C_{18}H_{17}CdN_5O_{10}$: C, 38.58; H, 3.04; N, 12.51. Found: C, 38.41; H, 3.12; N, 12.35.

X-ray Crystallography

X-ray single crystal structural data of **1** and **2** were collected on a Bruker Smart-CCD diffractometer equipped with a normal focus, 2.4 kW sealed tube X-ray source with graphite monochromated Mo-*Kα* radiation (λ = 0.71073 Å) operating at 50 kV and 30 mA. The program SAINT[14] was used for integration of diffraction profiles and absorption correction was made with SADABS[15] program. All the structures were solved by SIR 92[16] and refined by full matrix least square method using SHELXL-97.[17] All the hydrogen atoms were geometrically fixed and placed in ideal positions. The –NO_2 group of NO_2-bdc linker is in positional disorder in compound **2** and this has been resolved. Potential solvent accessible area or void space was calculated using the PLATON multipurpose crystallographic software.[18]All crystallographic and structure refinement data of **1** and **2** are summarized in Table 1. Selected bond lengths and angles for **1** and **2** are given in Table S2-S3 respectively. All calculations were carried out using SHELXL 97,[17] PLATON, SHELXS 97[19] and WinGX system, Ver 1.70.01.[20]

Adsorption Study

The adsorption isotherms of CO_2 (195 K), and N_2 (77 K) using the dehydrated sample of **1** and **2** were measured by using QUANTACHROME QUADRASORB-*SI*

analyzer. In the sample tube the adsorbent sample **1** and **2** (~100-150 mg) were placed which had been prepared at 353 and 393 K, respectively under a 1×10^{-1} Pa vacuum for about 6 h prior to measurement of the isotherms. Helium gas (99.999% purity) at a certain pressure was introduced in the gas chamber and allowed to diffuse into the sample chamber by opening the valve. The amount of gas adsorbed was calculated readily from pressure difference (P_{cal} - P_e), where P_{cal} is the calculated pressure with no gas adsorption and P_e is the observed equilibrium pressure. All operations were computer-controlled and automatic.

The adsorption of different solvents like MeOH at 293K and H_2O, EtOH at 298 K were measured in the desolvated sample of **1** and **2** in the vapour state by using BELSORP-aqua-3 analyzer. The samples of about ~ 100–150 mg were activated by similar conditions as mentioned earlier. The different solvent molecules used to generate the vapour were degassed fully by repeated evacuation. Dead volume was measured with helium gas. The adsorbate was placed into the sample tube, then the change of the pressure was monitored and the degree of adsorption was determined by the decrease in pressure at the equilibrium state. All operations were computer controlled and automatic.

Computational details

To find the position of a gas molecule inside MOF **1**, density functional theory calculations were carried out using the QUICKSTEP module in CP2K software.[21] All valence electrons were treated in a mixed basis set with an energy cut-off of 280 Ry. The short-range version of the double-ζ single polarization basis set was used. The effect of core electrons and nuclei was considered by using pseudo-potentials of Goedecker−Teter−Hutter (GTH).[22] The exchange and correlation interaction between electrons was treated with the Perdew−Burke−Ernzerhof (PBE)[23] functional. van der Waals interactions between the gas and the framework are very important,[24] their effects were accounted for by employing empirical corrections developed by Grimme. Two schemes, DFT-D2[25] and DFT-D3[26] were used to calculate the cell volume. Binding energy was calculated using PBE-D3 scheme. The simulation cell consisted of 1 × 1 × 1 unit cell for MOF. The optimized cell parameters are shown in supporting information Table S1.

Furthermore, to identify the favourable binding sites for CO_2 in 1 × 1 × 1 unit cell, Born-Oppenheimer Molecular Dynamics (BOMD) simulations were performed at a temperature of 50 K. The coordinates of the MOF were constrained during these run. The nuclear equations of motion were integrated using a standard velocity Verlet algorithm with a

time step of 0.5 fs. Canonical ensemble (NVT) trajectory was generated for 12 ps, with the temperature being maintained using a Nose-Hoover thermostat[27] using a coupling constant of 500 fs. Potential energy of the system is plotted as a function of time in Figure S1. Geometry optimization calculation was performed for the low energy configuration which was identified from MD trajectory. These runs were assumed to be converged when the maximum force on any atom was less than $1x10^{-4}$ a.u.

The binding energy of gas molecule (CO_2) is calculated using following formula

$$\Delta E = E(MOF\text{-}CO_2) - E(MOF) - n \times E(CO_2)$$

Where ΔE, $E(MOF\text{-}CO_2)$, E(MOF), E(CO2) and n are the binding energy of CO_2, energy of MOF with CO_2, energy of MOF, energy of CO_2 and n is the number of CO_2 molecules present in the MOF respectively. Binding energies of CO_2 were corrected for basis set superposition error using the counterpoise method.[28-29] All the structures were visualized in (VMD),[30] Mercury[31] and GaussView.[32]

Results and discussion

Crystal structure description of 1 and 2

Compound **1** crystallizes in monoclinic *C*2/*c* spacegroup (Table 1) and contains a distorted octahedral Cd(II) center coordinated by four oxygen atoms from three NH_2-bdc and two nitrogen atoms, one from NH_2-bdc and other one from bpe linker (Fig. 1a). Each NH_2-bdc chelates to a Cd(II) by one carboxylate group and connect another two Cd(II) centers through *syn-syn* bridging resulting in a 2D sheet like structure along *ab* plane (Fig. 1b). These 2D sheets are joined by the -NH_2 group of NH_2-bdc to form a 3D structure. These 2D sheets are further supported by bpe linkers and furnish 1D channels along the crystallographic *c*-axis. The square shaped channels (2.9×2.9 $Å^2$)[33] filled with ethanol guest molecules (Fig. 1c). Each of the NH_2-bdc linker acts as tetradentate chelating/bridging ligand and propagates in three directions and linking the Cd(II) centers with distance of 3.705 Å through *syn-syn* carboxylate bridging, 8.504 Å through NH_2-carboxylate bridging and 11.665 Å through the two carboxylate bridging at 1,4 positions. The Cd(II)-O bond lengths are in the range of 2.198(3)–2.546(2)Å and Cd(II)-N are in the range of 2.283(2)-2.376(3) Å (Table S2). After

removal of all solvent molecules available void space was found to be ~ 16 % of total cell volume, calculated using PLATON.[18] Topology analysis using TOPOS suggests a 3 nodal (2,4,5)-connected net with Schläfli symbol $\{4^3.6^2.8^5\}2\{4^3.6^2.8\}2\{8\}$ (Fig. 1d).[34]

Compound **2** crystalizes in orthorhombic *Cmma* spacegroup and the structural features are quite different from that of **1**. The primary changes in **2** from **1** are - NH_2-bdc and bpe linkers are replaced by NO_2-bdc and azbpy linkers respectively. Here the Cd(II) centers are six-coordinated distorted octahedral in nature, the equatorial positions are occupied by the two oxygen atoms (O1 and O1*) from one NO_2-bdc and two nitrogen atoms (N1 and N1*) from two azbpy linkers; the axial positions are filled by carboxylate oxygen atoms (O2 and O2*) from two NO_2-bdc linkers (Fig. 2a). Here the Cd(II) centers are connected by the carboxylate groups to form a linear chain along *c* direction (Fig. S2). These chains further connect to each other by the NO_2-bdc to form a ladder like 1D structure (Fig. 2b). These ladders are connected by azbpy linkers along *ab* plane to generate a 3D framework structure. View along *c* axis shows that the single net leaves a huge space of dimensions 18.5 × 14.7 $Å^2$ (Fig. 3a) and 3D framework undergoes two-fold interpenetration (Fig. 3b). View along *a* and *b*-axes show no space but a crown shaped 1D channel (6.5 × 5.3 $Å^2$)[33] can be viewed along *c* direction and these are occupied by guest water molecules (Fig. 3c-3d). The total void space calculated after guest solvent removal was found to be 32 % of total cell volume. Topology analysis using TOPOS suggests a 3 nodal (2,3,5)-connected net with Schläfli symbol $\{4^2.6.8^4.10^2.12\}\{4^2.6\}\{8\}$.

Framework stability and PXRD analysis:

Thermogravimetric analysis of compound **1** shows initial weight loss of 6 wt% at 55 °C which corresponds to loss of guest ethanol molecule (Fig. S3). From 60 - 400 °C the desolvated framework is stable and further increase in temperature decomposes the framework structure. The PXRD pattern of desolvated framework is very similar to that of as-synthesized pattern (Fig. 4a). Indexing of the dehydrated PXRD pattern of **1** reveals similar cell parameter as of as-synthesized **1** suggesting the framework is rigid in nature. Compound **2**, loses all the guest water molecules at 110 °C and is stable till 350 °C. Further heating leads to decomposition of the framework (Fig. S3). The PXRD pattern of the desolvated **2** (**2′**) shows distinct changes compared to that of the as-synthesized framework suggesting structural transformation after dehydration. Indexing of the powder pattern of desolvated framework shows that the Braggs' reflection corresponding to (010) plane which

passes through the azbpy shifts to higher angle and also there are significant changes in cell parameters along *b*-and *c*-axis (Desolvated 2 cell parameters: a = 6.7227 Å, b = 9.5213 Å, c = 24.7736 Å). Hence this can be attributed to the structural reorganization of the framework after dehydration (Fig. 4b and S4).

Gas and solvent vapour adsorption

To check the porous properties of compound **1**, we measured N_2 adsorption isotherm at 77 K which showed type-II profile indicating only surface adsorption (Fig. 5). Considering the kinetic diameter of N_2 (3.64 Å),[35] diffusion into the pores is not possible due to smaller pore diameter. Surprisingly, at 195 K we observed a type-I CO_2 (3.3 Å) uptake profile with total uptake of ~ 39 mLg^{-1} (~7.6 wt %) (Fig. 5). The Langmuir surface area was calculated to be 245 m^2g^{-1}. Moreover, the desorption path does not coincidence with adsorption and exhibits a prominent hysteretic sorption profile. Calculation of isosteric heat of adsorption using Dubinin–Radushkevich (DR) equation shows an appreciably high value of 35.9 $kJmol^{-1}$, which indicates stronger binding of CO_2 with framework **1′**.[36] Diffusion of CO_2 is possible due to its smaller kinetic diameter and also its high quadrupole moment that can interact with the π cloud of the aromatic rings on the pore surface.

To understand and to obtain an insight of the CO_2 adsorption phenomenon, density functional theory calculations were carried out. Initially the solvent removed **1** was considered and cell parameters were optimized using PBE, PBE-D2 and PBE-D3 methods. These results are given in Table S1.The optimal position of CO_2 is shown in Fig.6a. Binding energy of one CO_2 with the MOF was calculated as -40.22 $kJmol^{-1}$. Further, electron density difference maps have been calculated to understand the nature of interactions exhibited by CO_2 with framework molecular groups. This is calculated using the relation,

$$\Delta\rho = \rho(\text{MOF-CO}_2) - \rho(\text{MOF}) - \rho(\text{CO}_2)$$

Where $\Delta\rho$, $\rho(\text{MOF-CO}_2)$, $\rho(\text{MOF})$ and $\rho(\text{CO}_2)$ are the electron density difference of the system, total electron density of MOF with CO_2, individual electron density of MOF and isolated CO_2 respectively. This map is shown in Fig. 6b. Blue and lime colors indicate increased and decreased electron densities, respectively; the chief interaction is one involving the π systems of CO_2 and of the aromatic molecular groups of linkers in MOF. CO_2 molecule interacts with two phenyl and two pyridine molecular groups. It lies nearly equidistant from the four aromatic rings of the MOF at distances of 3.50, 3.55, 3.60 and 3.66 Å from the C

atom of the rings as shown in Fig.6a and 6b. Assuming that CO_2 interacts with all these four aromatic molecular groups equally strongly, the binding energy per phenyl ring or pyridine ring is approximately 10 $kJmol^{-1}$. This value is consistent with the strength of the π-π interaction between CO_2 and phenyl or pyridine molecular groups determined using quantum chemical calculations (MP2) as reported in the literature. Theoretically, six CO_2 molecules can be accommodated within the framework, which matches well the maximum number of CO_2 molecules in a unit cell obtained from experimental adsorption measurement. The optimized positions of all CO_2 molecules as per the maximum loading are shown in Fig. 7. The binding energy of CO_2 in such a fully loaded MOF was calculated to be 33.40 $kJmol^{-1}$.

We further carried out water and methanol vapour adsorption experiments at 298 and 293 K, respectively (Fig. 8). The water vapour uptake increases almost linearly with pressure and saturates at 55 mLg^{-1} and a very small hysteresis can be found. This suggests very moderate interaction with the pore surface as from the crystal structure it is evident that the pore surface is mostly hydrophobic due to the presence of aromatic rings. The MeOH sorption profile suggests gradual and small uptake (27 mLg^{-1}) and this can be attributed to the larger kinetic diameter of MeOH.

Compound **2′** does not show any uptake of N_2 at 77 K, as the desolvated form possibly undergoes structural contraction and hence the pore window is not sufficient for N_2 diffusion (Fig. S5). At 195 K, we observed a very small uptake (15 mLg^{-1}) of CO_2 as the pore dimension is possibly not suitable for CO_2 and also unavailability of any interaction sites (Fig. S6). But **2′** adsorbs different solvent vapours and shows interesting structural rearrangement characteristics. At 298 K, the water vapour adsorption profile reveals a gate opening type profile; till $P/P_0 \sim 0.2$ there is almost no uptake but suddenly the uptake profile rises steeply to reach a saturation value of 185 mLg^{-1} which corresponds to 4 molecules of H_2O per formula (Fig. 9). This sort of behaviour reveals presence of hydrophobic as well as hydrophilic sites in the pore surface. The notion of dual sites is further evidenced from the methanol and ethanol vapour adsorption profiles. The final uptake amount of methanol and ethanol are 84 and 54 mLg^{-1} (1.85 and 1.2 molecules of methanol and ethanol per formula, respectively), respectively which are much less compared to amount of water uptake and also in accordance with molecular sizes (Fig. 9). Both the profiles show stepwise uptake[37] at very low relative pressures. For methanol, at $P/P_0 \sim 0.018$ and for ethanol $P/P_0 \sim 0.027$ we can see a sudden rise in the uptake amounts and these can be considered as structural rearrangement assisted by the guest molecules. Evidently presence of hydrophobic sites acts strongly to

allow the diffusion of methanol and ethanol, whereas water molecule having smaller kinetic diameter is unable to diffuse at very low pressure.

In conclusion, we have synthesized two new 3D porous MOFs of Cd(II) with functionalized organic linkers, NH_2-bdc and NO_2-bdc. Framework **1** with coordinated -NH_2 functional group is found to be rigid upon desolvation and shows selective uptake of CO_2 at 195 K. From DFT calculations we realized that the CO_2 molecules interact with the aromatic rings at the pore surfaces and it renders a moderate heat of adsorption. Framework **2** contains pendent –NO_2 groups at the pore surfaces and found to undergo structural rearrangement upon desolvation. This structural change renders hydrophobicity in the pore surfaces realized by water vapour adsorption studies. These results demonstrate that by simple change in the additional functional groups of the organic linkers could allow the structural modulation and associated porous properties.

Table 1: Crystal data and structure refinement parameters of compound **1** and **2**.

Parameters	1	2
empirical formula	$C_{30}H_{27}Cd_2N_4O_9$	$C_{18}H_{10}CdN_5O_{10}$
M	812.36	583.96
Cryst. system	Monoclinic	Orthorhombic
space group	*C*2/*c* (No. 15)	*Cmma* (No. 67)
a (Å)	16.3552 (6)	6.7119(7)
b (Å)	16. 0035(6)	24.876(3)
c (Å)	12.1024(5)	14.0647(17)
α (deg)	90	90
β (deg)	111.3990(10)	90
γ (deg)	90	90
V (Å^3)	2949.3(2)	2348.3(5)
Z	4	4
T(K)	293	150
λ (Mo K_α)	0.71073	0.71073
D_c (g cm^{-3})	1.830	1.586
μ (mm^{-1})	1.504	0.988
θ_{max} (deg)	27.28	25.0
total data	19039	8378
unique reflection	3316	1121
R_{int}	0.056	0.090
data [$I > 2\sigma(I)$]	2817	948
R^a	0.0295	0.0953
$R_w{}^b$	0.0682	0.2410
GOF	1.03	1.06

Acknowledgement

We thank Mrs. S. T. Cyriac for carrying out some of the experiments. R. H acknowledges DST, JNCASR, India. P. K and S. B acknowledge CSIR, India. S. B acknowledges the Centre for Development of Advanced Computing (C-DAC), Bangalore, for providing computational resources. T. K. M acknowledges Sheikh Saqr fellowship.

Electronic supplementary information (ESI) available: Selected bond distances for all compounds, crystal structure figures and Indexing results. Crystallographic files for compounds **1** and **2** in cif format.

References:

1. (*a*) S. Kitagawa, R. Kitaura and S. Noro, *Angew Chem. Int. Ed*., 2004, **43**, 2334; (*b*) L. Song, J. Zhang, L. Sun, F. Xu, F. Li, H. Zhang, X. Si, C. Jiao, Z. Li, S. Liu, H, Zhou, D. Sun, Y, Du, Z, Cao and Z. Gabelica, *Energy Environ Sci*., 2012, **5**, 7508; (*c*) M. Eddaoudi, J. Kim, N. L. Rosi, D. T. Vodak, J. Wachter, M. O'Keeffe and O. M. Yaghi, *Science*., 2002, **295**, 469; (*d*) M. Eddaoudi, H. Li and O.M. Yaghi, *J. Am. Chem. Soc.,* 2009,**131**, 8376; (*e*) Y. He, R. Krishna and B. Chen, *Energy Environ Sci*. 2012, **5**, 9107.
2. (*a*) R. K. Motkuri, J. Tian, P. K. Thallapally, C. A. Fernandez, S. J. Dalgarno, J. E. warren, B. P. McGrail and J. L. Atwood, *Chem. Commun*. 2010, **46**, 538; (*b*) J.-R. Li, R. J. Kuppler and H. -C. Zhou, *Chem. Soc. Rev*. 2009, **38**, 1477; (*c*) J.-R. Li, J. Sculley and H. -C. Zhou, *Chem. Rev*. 2012, **112**, 869;
3. (*a*) J. Y. Lee, O. K. Farha, J. Roberts, K. A. Scheidt, S. T. Nguyen and J. T. Hupp, *Chem. Soc. Rev*. 2009, **38**, 1450; (*b*) S. Hasegawa, S. Horike, R. Matsuda, S. Furukawa, K. Mochizuki, Y. Kinoshita and S. Kitagawa, *J. Am. Chem. Soc*. 2007, **129**, 2607; (*c*) R. Haldar, S. K. Reddy, V. M. Suresh, S. Mohapatra, S. Balasubramanian and T. K. Maji, *Chem. Eur. J*. 2014, DOI:10.1002/chem.201303610; (*d*) R. Q. Zou, H. Sakurai and Q. Xu, *Angew Chem. Int. Ed*., 2006, **45**, 2542.
4. (*a*) B. Chen, S. Xiang and G. Qian, *Acc Chem. Res*, 2010, **43**, 1115; (*b*) K. Jayaramulu, R. P. Narayan, S. J. George and T. K. Maji, *Inorg. Chem*. 2012, **51**, 10089; (*c*) S. Mohapatra, S. Adhikari, H. Riju and T. K. Maji, Inorg. Chem., 2012, **51**, 4891; (d) S. S. Nagarkar, B. Joardar, A. K. Chaudhari, S. Mukherjee and S. K. Ghosh, *Angew. Chem., Int. Ed*. 2013, **52**, 2881; (*e*) B. Manna, A. K. Chaudhari, B. Joardar, A. Karmakara and S. K. Ghosh, *Angew. Chem., Int. Ed*. 2013, **52**, 998.
5. (*a*) Y. Cui, Y. Yue, G. Qian and B. Chen, *Chem. Rev*. 2012, **112**, 1126; (*b*) V. M. Suresh, S J. George and T. K. Maji, *Adv. Funct. Mater*, 2013, **23**, 5585; (*c*) M. –J. Dong, M. Zhao, S. Ou, C. Zou and C. –D. Wu, *Angew. Chem., Int. Ed*. 2013, **52**, 1; (d) P. Falcaro, D. Buso, A. J. Hill and C. M. Doherty, *Adv. Mater*. 2012, **24**, 3153.
6. (*a*) R. Haldar and T. K. Maji, *CrystEnggComm*, 2012, **14**, 684; (*b*) R. Haldar and T. K. Maji, *CrystEnggComm*, 2013, **15**, 9276; (*c*) S. Henke, A. Schneemann, A. Wütscher and R. A. Fischer, *J. Am. Chem. Soc*. 2012, **134**, 9464; (*d*) S. Henke, R.

Schmid, J.-R. Grunwaldt and R. A. Fischer, *Chem. Eur. J*. 2010, **16**, 14296; (*e*) A. Thirumurugan and S. Natarajan, *Dalton. Trans*. 2004, **18**, 2923.

7. M. H. Alkordi, Y. Liu, R. W. Larsen, J. F. Eubank and M. Eddaoudi, *J. Am. Chem. Soc*. 2008, **130**, 12639.
8. A. Goursot, V. Vasilyev and A. Arbuznikov, *J. Phys. Chem. B*. 1997, **101**, 6420.
9. H. Furukawa, K. E. Cordova, M. O'Keeffe and O. M. Yaghi, *Science*, 2013, **341**, 1230444.
10. (*a*) R. Vaidhyanathan, S. S. Iremonger, G. K. H. Shimizu, P. G. Boyd, S. Alavi and T. K. Woo, *Science*. 2010, **330**, 650; (*b*) T. M. McDonald, W. R. Lee, J. A. Mason,B. M. Wiers, C. S. Hong and J. R. Long, *J. Am. Chem. Soc.* 2012, **134**, 7056; (*c*) W. Lu, J. P. Scully. D. Yuan, R. Krishna, Z. Wei and H. –C. Zhou, *Angew. Chem., Int. Ed*. 2012, **51**, 1; (*d*) M. H. Mohamed, S. K. Elsaidi, L. Wojtas, T. Pham, K. A. Forrest, B. Tudor, B. Space and M. J. Zaworotko, *J. Am. Chem. Soc.* 2012, **134**, 19556; (*e*) S. D. Burd, S. Ma, J. A. Perman, B. J. Sikora, R. Q. Snurr, P. K. Thallapally, J. Tian, L. Wojtas and M. J. Zaworotko, *J. Am. Chem. Soc.* 2012, **134**, 3663; (*f*) P. Negent, Y. Belmabkhout, S. D. Burd, A. J. Cairns, R. Luebke, K. Forrest, T. Pham, S. Ma, B. Space, L. Wojtas, M. Eddaoudi and M. J. Zaworotko, *Nature*, 2013, **495**, 80; (*g*) D. Britt, H. Furukawa, B. Wang, T. G. Glover and O. M. Yaghi, *Proc. Natl. Acad. Sci. USA*, 2009, **106**, 20637.
11. (*a*) P. Kar, R. Biswas, Y. Ida, T. Ishida and A. Ghosh, *Cryst Growth Des*. 2011, **11**, 5305; (*b*) J. Long, S. Wang, Z. Ding, S. Wang, Y. Zhou, L. Huang and X. Wang, *Chem. Commun*. 2012, **48**, 11656; (*c*) P. Falcaro, F. Lapierre, B. Marmiroli, M. Styles, Y. Zhu, M. Takahashi, A. J. Hill and C. M. Doherty, *J. Mater. Chem. C*, 2013, **1**, 42; (*d*) Y. Huang, Z. Zheng, T. Liu, J. Lu, Z. Lin, H. Li and R. Cao, *Catal. Commun*, 2011, **14**, 27.
12. (*a*) P. Kanoo, S. K. Reddy, G. Kumari, R. Haldar, C. Narayana, S. Balasubramanian and T. K. Maji, *Chem. Commun*. 2012, **48**, 8487; (*b*) K. Jayaramulu, S. K. Reddy, A. Hazra, S. Balasubramanian and T. K. Maji, *Inorg. Chem*. 2012, **51**, 7103; (*c*) C. M. Nagaraja, R. Haldar, T. K. Maji and C. N. R. Rao, *Cryst Growth Des*. 2012, **12**, 975; (*d*) P. Kanoo, A. C. Ghosh, S. T. Cyriac and T. K. Maji, *Chem. Eur. J*. 2012, **18**, 237.
13. E. V. Brown and G. R. Granneman, *J. Am. Chem. Soc.*, 1975, **97**, 621.
14. SMART (V 5.628), SAINT (V 6.45a), XPREP, SHELXTL; Bruker AXS Inc. Madison, Wisconsin, USA, 2004.

15. G. M. Sheldrick, Siemens Area Detector Absorption Correction Program, University of Götingen, Götingen, Germany, 1994.
16. A. Altomare, G. Cascarano, C. Giacovazzo and A. Gualaradi, *J. Appl. Cryst*,. 1993, **26**, 343.
17. G. M. Sheldrick, SHELXL-97, Program for Crystal Structure Solution and Refinement; University of Götingen, Götingen, Germany, 1997.
18. A. L. Spek, *J. Appl. Crystallogr*., 2003, **36**, 7.
19. G. M. Sheldrick, SHELXS 97, Program for the Solution of Crystal Structure, University of Götingen, Germany, 1997.
20. L. J. Farrugia, WinGX-A Windows Program for Crystal Structure Analysis, *J. Appl. Cryst.*, 1999, **32**, 837.
21. (*a*) J. VandeVondele, M. Krack, F. Mohamed, M. Parrinello, T. Chassaing and J. Hutter, *Comput. Phys. Commun.* 2005, **167**, 103; (*b*) J. Hutter, M. Iannuzzi, F. Schiffmann and J. VandeVondele, *Wiley Interdiscip. Rev.: Comput. Mol. Sci.* 2013, DOI: 10.1002/wcms.1159.
22. M. Elstner, D. Porezag, G. Jungnickel, J. Elsner, M. Haugk, T. Frauenheim, S. Suhai and G. Seifert, *Phys. Rev. B.* 1998, **58**, 7260.
23. J. P. Perdew, K. Burke and M. Ernzerhof, *Phys. Rev. Lett*. 1996, **77**, 3865.
24. A. Hazra; S. Bonakala, S. K. Reddy, S. Balasubramanian and T. K. Maji, *Inorg. Chem*, 2013, **52**, 11385.
25. S. Grimme, *J. Comput. Chem*. 2006, **27**, 1787.
26. S. Grimme, J. Antony, S. Ehrlich and H. Krieg, *J. Chem. Phys*. 2010, **132**, 154104
27. (*a*) S. Nose, *J. Chem. Phys*, 1984, **81**, 511; (b) S. Nose, *Mol. Phys*, 1984, **52**, 255.
28. H. B. Jansen and P. Ros, *Chem. Phys. Lett*. 1969, **3**, 140.
29. B. Liu and A. D. McLean, *J. Chem. Phys*. 1973, **59**, 4557.
30. W. Humphrey, A. Dalke and K. Schulten, *J. Mol. Graphics.* 1996, **14**, 33.
31. (*a*) Mercury - Crystal Structure Visualisation and Exploration Made Easy. http://www.ccdc.cam.ac.uk/products/mercury/ (accessed June 18, 2010); (*b*) C. F. Macrae, P. R. Edgington, P. McCabe, E. Pidcock, G. P. Shields, R. Taylor, M. Towler, J. Van de Streek, *J. Appl. Crystallogr.* 2006, **39**, 453.
32. GaussView, Version 5.0, Roy Dennington, Todd Keith and John Millam, Semichem Inc., Shawnee Mission KS, 2009.
33. The sizes of the channels were calculated considering the van der Waals radii of the atoms.

34. A. L. Spek, *J. Appl. Crystallogr*. 2003, **36**, 7.

35. C. E. Webster, R. S. Drago and M. C. Zerner, *J. Am. Chem. Soc*., 1998, **120**, 5509.

36. M. M. Dubinin, *Chem. Rev.,* 1960, **60**, 235.

37. Z. Zhang, S. Xiang, X. Rao, Q. ZhengF. R. FronczekG. Qian and B. Chen, *Chem. Commun*. 2010, **46**, 7205.

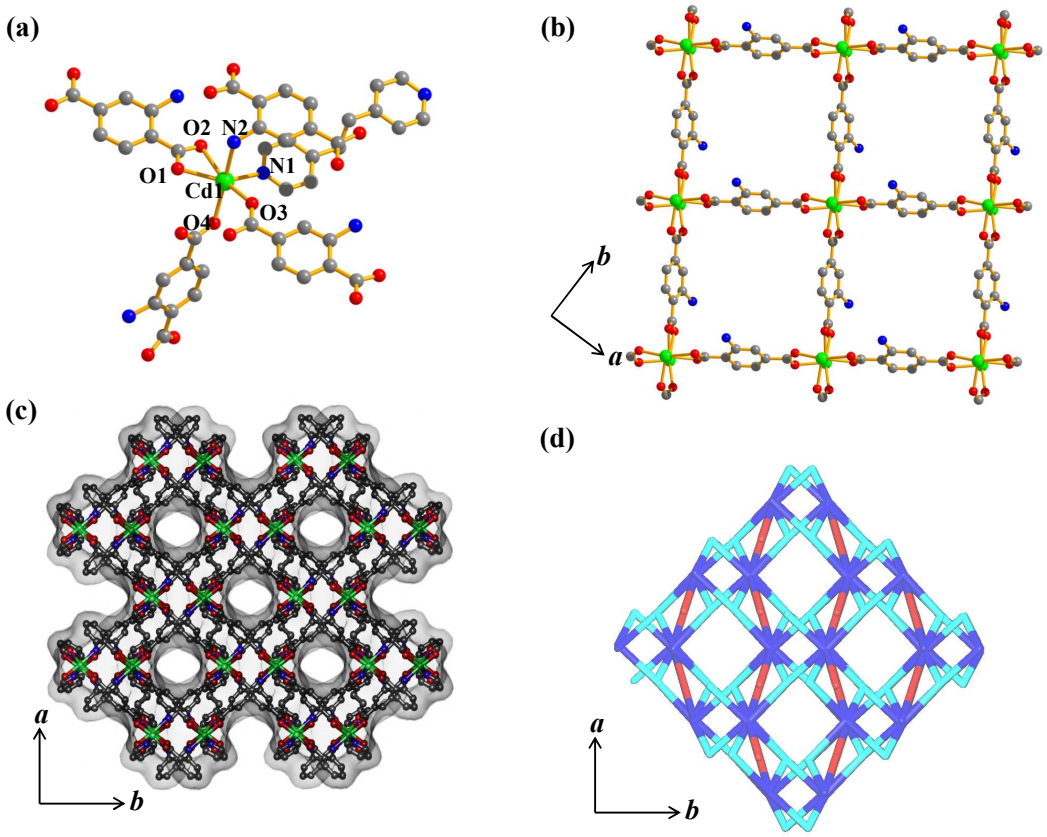

Fig. 1: (a)View of the Cd(II) coordination sphere in compound **1**; (b) View of the 2D sheet along *ab* plane; (c) Distorted square shaped pore along *c*-axis; (d) View of the 3D net along *c*-axis.

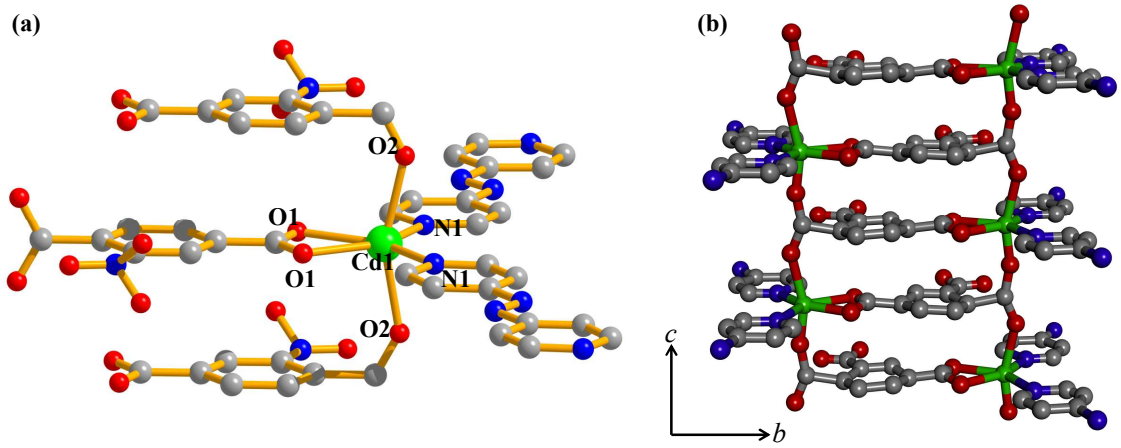

Fig. 2: (a) View of the coordination environment of Cd(II) in compound **2**; (b) Ladder-like 1D structure formed by NO_2-bdc and Cd(II) in **2**.

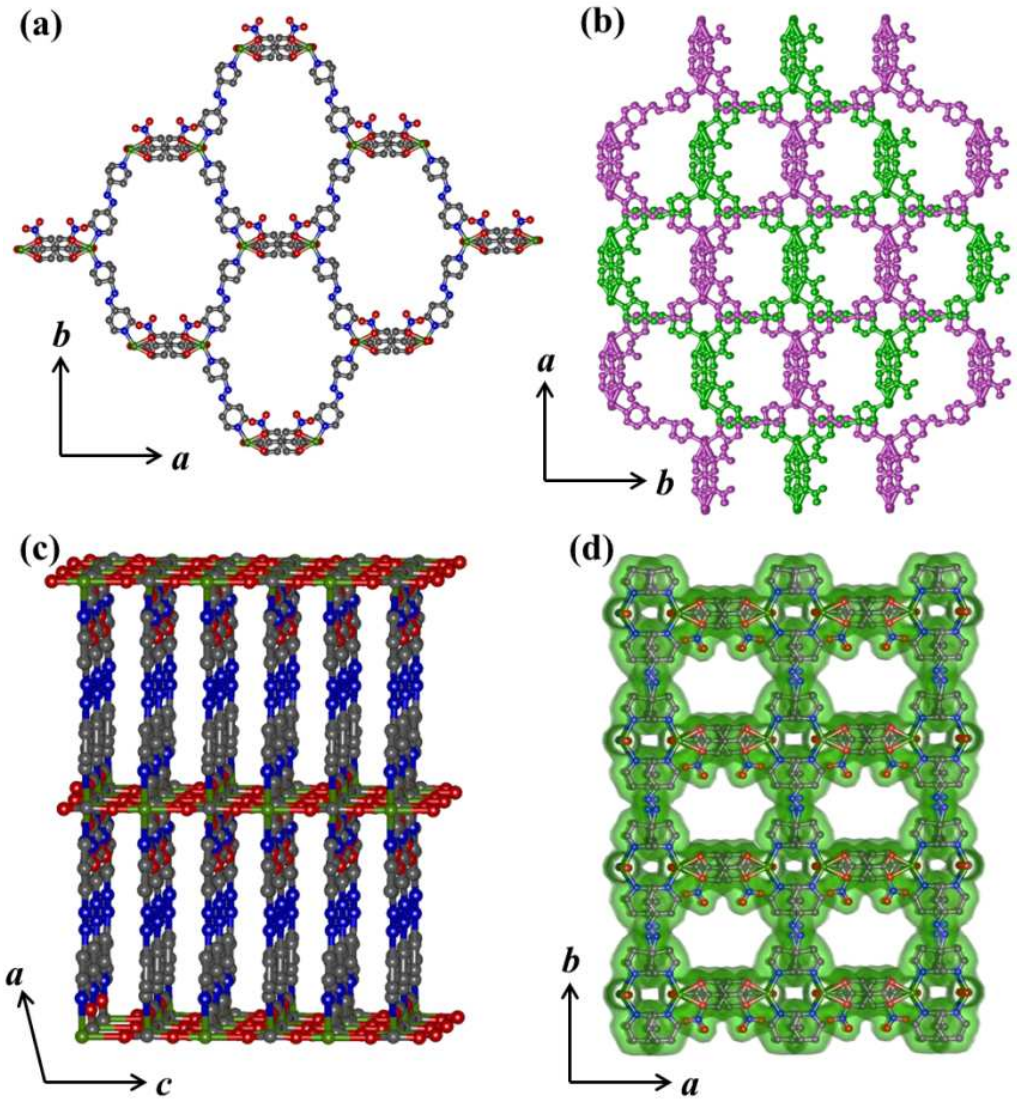

Fig. 3: (a) View of the single net in compound **2**; (b) View of the two-fold interpenetrated nets along *c*-axis; (c) View of the 3D framework along *b*-axis; (d) View of the crown shaped pore window along *c*-axis.

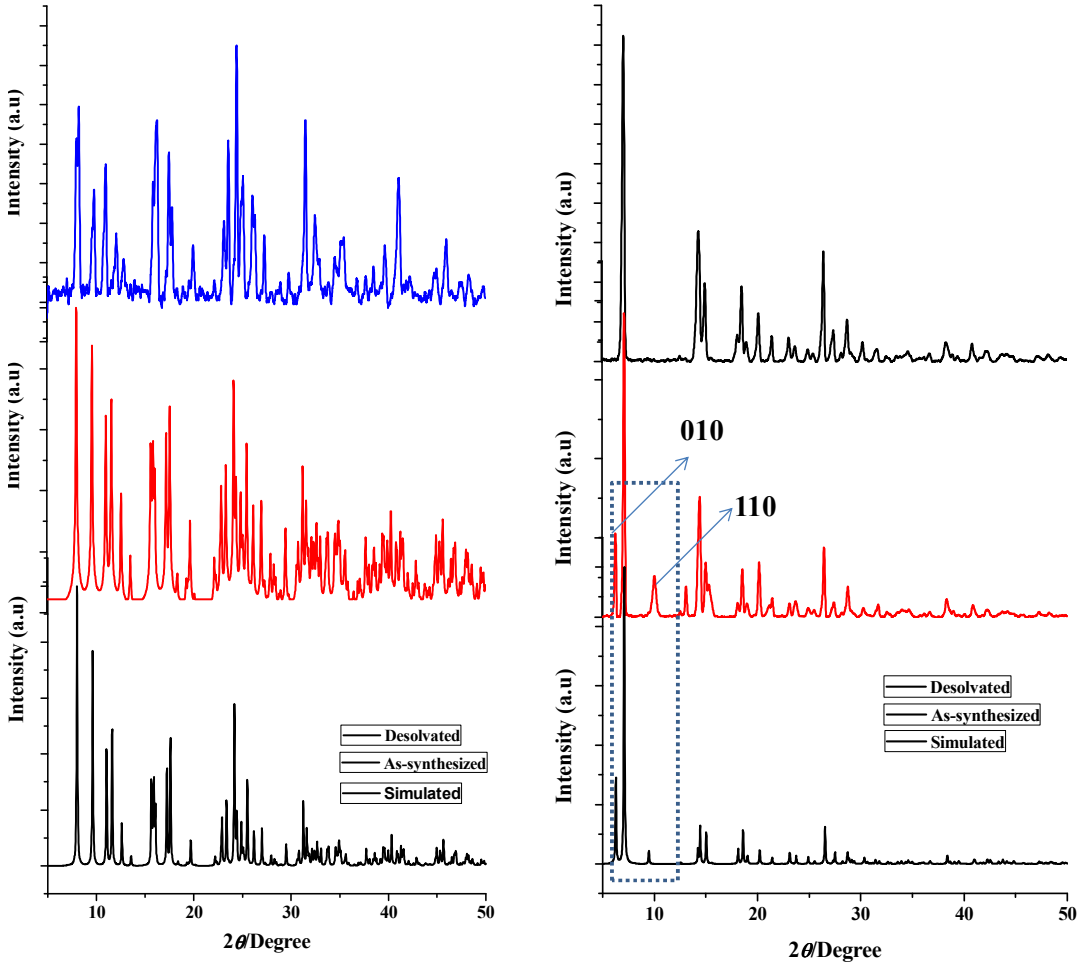

Fig. 4: PXRD patterns of (a) compound **1** and (b) compound **2**.

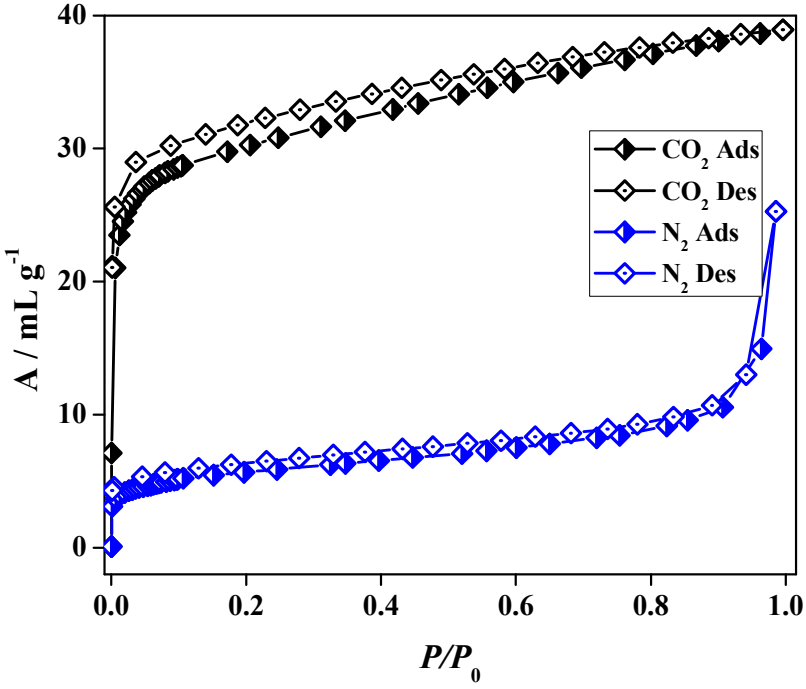

Fig. 5: N_2 and CO_2 adsorption profiles of **1′** at 77 and 195 K.

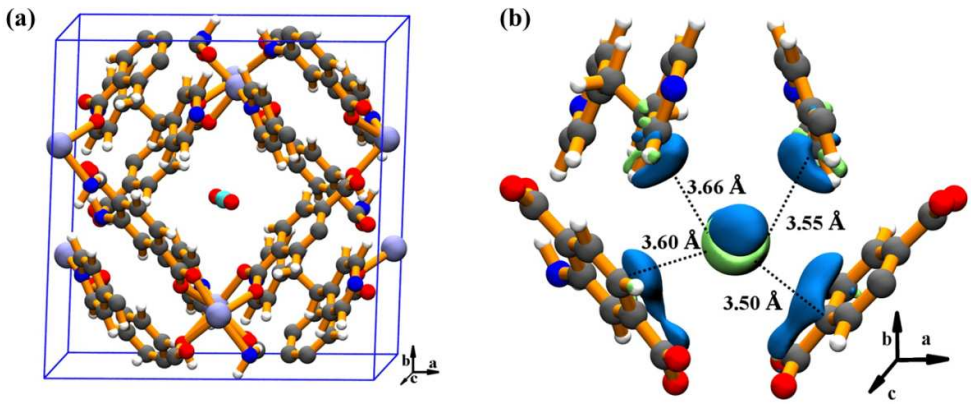

Fig. 6: (a) Location of CO_2 molecule inside **1′**, (b) Electron density difference map of CO_2 in **1′**. CO_2 interacts with aromatic molecular groups. Blue and lime color indicate the increased and decreased electron densities brought about by the adsorption of CO_2 in **1**, respectively. The view is along the crystallographic *c*-axis and the isosurface value is 10^{-4}a.u. The electron density difference has been calculated for the entire MOF. However, only the region around CO_2 is shown for clarity. Color scheme: MOF atoms- C-grey, N-blue, H-white, Cd-ice blue; CO_2 atoms: C-cyan, O-Red.

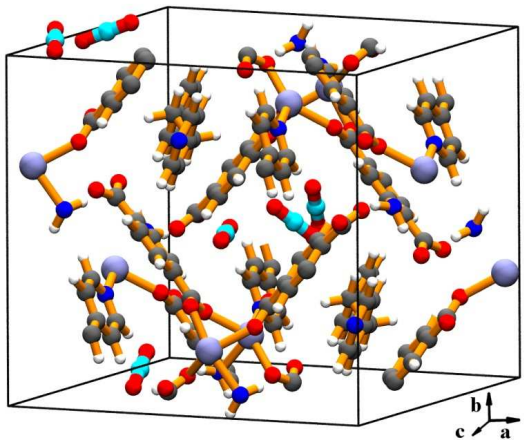

Fig. 7: Locations of CO_2 molecules in a fully loaded **1**. View along crystallographic *c*-axis. Color scheme: MOF atoms- C-gray, N-blue, H-white, Cd-ice blue; CO_2 atoms: C-cyan, O-Red.

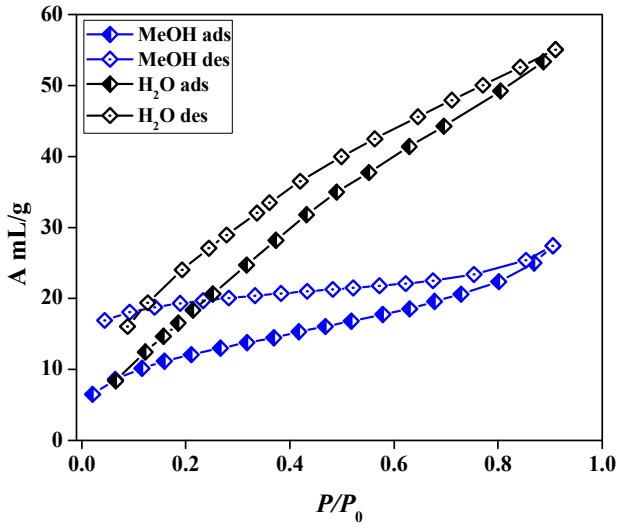

Fig. 8: Water and methanol vapour adsorption profiles for compound **1** at 298 and 293 K, respectively.

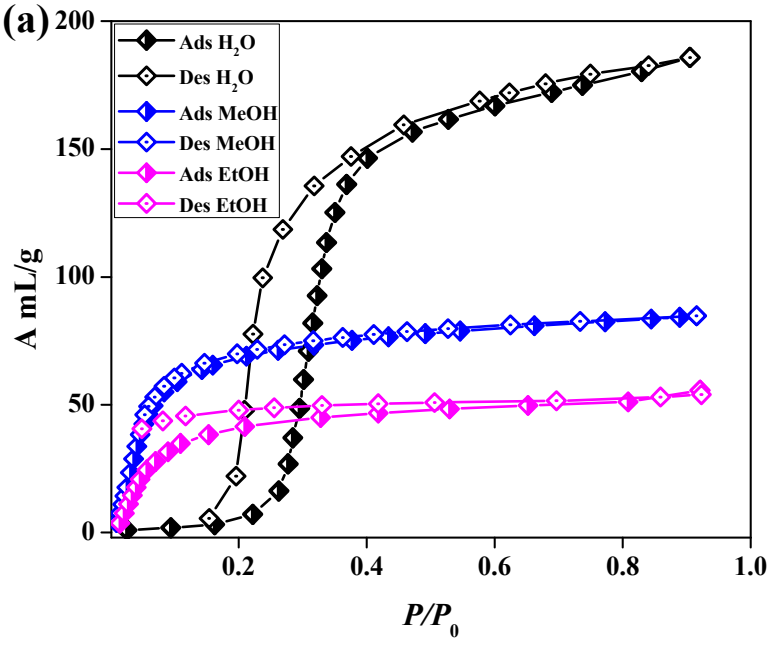

Fig. 9: H_2O (298 K), MeOH (293 K) and EtOH (298 K) vapour adsorption profiles of compound **2′**.

Table of Content

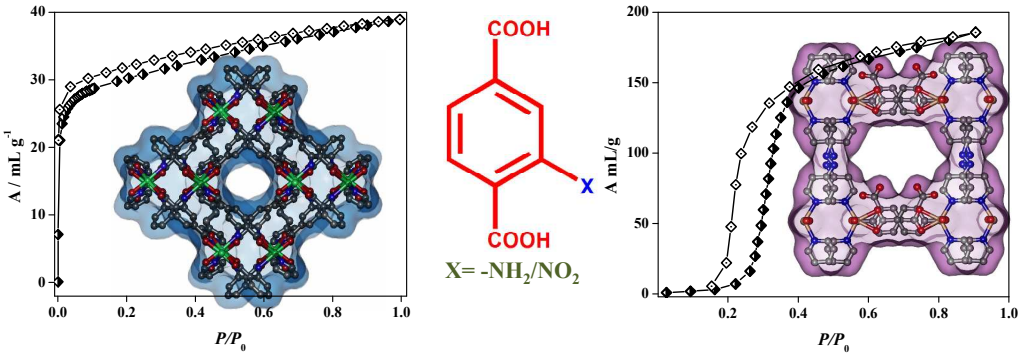

Selective CO_2 adsorption *Hydrophobic Pore*

Two Cd(II) based 3D frameworks show interesting structural features and adsorption properties based on the linker functionality modulation.